

What Are Special About Ground-Level Events? Flares, CMEs, Active Regions and Magnetic Field Connection

N.V. Nitta · Y. Liu · M.L. DeRosa · R.W. Nightingale

Received: 29 January 2011 / Accepted: 20 March 2012 / Published online: 21 April 2012
© Springer Science+Business Media B.V. 2012

Abstract Ground level events (GLEs) occupy the high-energy end of gradual solar energetic particle (SEP) events. They are associated with coronal mass ejections (CMEs) and solar flares, but we still do not clearly understand the special conditions that produce these rare events. During Solar Cycle 23, a total of 16 GLEs were registered, by ground-based neutron monitors. We first ask if these GLEs are clearly distinguishable from other SEP events observed from space. Setting aside possible difficulties in identifying all GLEs consistently, we then try to find observables which may unmistakably isolate these GLEs by studying the basic properties of the associated eruptions and the active regions (ARs) that produced them. It is found that neither the magnitudes of the CMEs and flares nor the complexities of the ARs give sufficient conditions for GLEs. It is possible to find CMEs, flares or ARs that are not associated with GLEs but that have more extreme properties than those associated with GLEs. We also try to evaluate the importance of magnetic field connection of the AR with Earth on the detection of GLEs and their onset times. Using the potential field source surface (PFSS) model, a half of the GLEs are found to be well-connected. However, the GLE onset time with respect to the onset of the associated flare and CME does not strongly depend on how well-connected the AR is. The GLE onset behavior may be largely determined by when and where the CME-driven shock develops. We could not relate the shocks responsible for the onsets of past GLEs with features in solar images, but the combined data from the Solar TERrestrial Relations Observatory (STEREO) and the Solar Dynamics Observatory (SDO) have the potential to change this for GLEs that may occur in the rising phase of Solar Cycle 24.

Keywords Sun: active regions · Sun: particle emission · Sun: magnetic field

N.V. Nitta (✉) · M.L. DeRosa · R.W. Nightingale
Dept./ADBS, B/252, Lockheed Martin Solar and Astrophysics Laboratory, 3251 Hanover Street,
Palo Alto, CA 94304, USA
e-mail: nitta@lmsal.com

Y. Liu
Stanford University, Stanford, 94305, USA

1 Introduction

Ground-level events (GLEs) are a special class of solar energetic particle (SEP) events, in which ions are accelerated to relativistic energies and cause ground-level effects. As of the second half of 2011, there have been only 70 GLEs on record since 1942, including 16 during Solar Cycle 23 (Gopalswamy et al. 2010, 2012). Though detailed case studies have been conducted on a number of individual GLEs, we still do not fully understand the conditions and processes that are responsible for these extreme SEP events.

With a high ~ 10 MeV proton flux, GLEs are usually identified with so-called gradual (as opposed to impulsive) SEP events, which are accelerated at shocks driven by coronal mass ejections (CMEs) (e.g., Reames 1999; Kahler et al. 2011b). Another view, however, is that some GLEs come directly from solar flares, which may also accelerate particles to high energies in magnetic reconnection, primarily because their temporal variations mimic those of impulsive flares (Grechnev et al. 2008; McCracken et al. 2008). Aschwanden (2012) also argued that, in five of the 13 GLEs he studied, the particles are released during the impulsive phase of the associated flare. However, it could be problematic to advocate the flare origin of GLEs on the basis of temporal variations alone, because the flare impulsive phase tends to be contemporaneous with the CME rapid acceleration phase (Zhang et al. 2001; Temmer et al. 2010), which may be the likeliest time for the formation of a shock wave. In addition, direct contributions of flare-accelerated particles in GLEs may be suggested by the SEP compositions and charge states similar to those of impulsive SEP events (see, e.g., Cohen et al. 1999, for GLEs 55–57).

GLEs tend to be associated with fast CMEs and intense flares (e.g., Gopalswamy et al. 2010, 2012, and Sect. 2). Apart from the magnitudes of the associated CMEs and flares, there seem to be at least two more factors that may contribute to large SEP events in near-Earth space including GLEs. One is the presence of prior CMEs. Gopalswamy et al. (2004) showed statistically that large SEP events tend to be associated with CMEs preceded by another CME from the same region within a 24 hour time window. Similar conclusions were reached by Kahler and Vourlidis (2005). The preceding CME may perform pre-conditioning in two ways: to provide seed particles to be re-accelerated at the shock driven by the main CME (Kahler 2001; Cliver et al. 1983; Cliver 2006), and to cause higher level of turbulence in the upstream region of the main CME (Li and Zank 2005). Recently Li et al. (2011) have further developed the concept of double CMEs occurring close in time that may lead to enhanced particle acceleration.

Another factor is magnetic field connection of the acceleration region to Earth. The source regions of gradual SEP events, usually active regions (ARs), are distributed in much broader longitudes than those of impulsive SEP events (Reames 1999), presumably reflecting larger extensions of the CME-driven shocks than the reconnection regions above flares. The broad longitudinal distribution of source ARs may discount the importance of their magnetic field connection to the observer. However, the time profiles of gradual SEP events depend on the source longitudes. For example, those from the western source ARs tend to rise more quickly to the peak than those from the eastern source regions (Cane et al. 1988, 2003; Reames 1999). This indicates that magnetic field connection of the source region and surrounding area may play a role in the SEP onset and peak times and possibly in other SEP properties, given that the western hemisphere is more likely connected to Earth in normal interplanetary conditions. Note that the very intense GLE on 20 January 2005 was associated with a flare around the longitude of W60.

Therefore the origin of large SEP events including GLEs may not be understood properly from the associated discrete solar events alone. Nevertheless, it is still meaningful to ask if

there are special properties of the flares and CMEs that are associated with GLEs, as well as of the ARs that produce them. In particular, the properties of ARs have only rarely been discussed with regard to large SEP events since space-borne solar data became routinely available in the 1990s (e.g., Nitta et al. 2003b; Gopalswamy et al. 2005a; Kahler et al. 2011b), and so we choose them as one of the central themes here.

This article is organized as follows. In Sect. 2, we discuss possible problems in defining and characterizing GLEs. We consider this to be important to set the scope of the following sections. In Sect. 3, we review the magnitudes of the flares and CMEs that were associated with GLEs in Solar Cycle 23. Section 4 compares some basic properties of the ARs that produced GLEs with those of (a) ARs that produced SEP events but not GLEs, and of (b) complex ARs in general. In Sect. 5, we discuss magnetic field connection of the source ARs and surrounding regions with Earth. We describe in Sect. 6 possible signatures of shocks that may be relevant to the onset of GLE events. We discuss and summarize this study in Sect. 7. Many topics, although possibly important, have to be excluded, such as cross field diffusion and the effect of prior CMEs and seed particles.

2 Problems in defining and characterizing GLEs

GLEs consist of relativistic ions. Like galactic cosmic-rays, they penetrate into Earth's atmosphere and produce secondary particles. The 16 GLEs registered during Solar Cycle 23 are summarized in Table 1. Whether a given SEP event is a GLE depends on the detection of the secondary particles usually by neutron monitors (NMs) at cosmic ray stations. For a given GLE, different NMs show different time profiles (e.g., Bieber et al. 2002; McCracken et al. 2008; Moraal and McCracken 2011), because of different asymptotic look angles and rigidities of the NMs combined with anisotropy of the particles.

Therefore, even though the onset time and maximum intensity in Table 1 (columns 3 and 4) are based on data from the Oulu Cosmic Ray Station (with a ≈ 0.8 GV cutoff rigidity)¹ as was the case with Gopalswamy et al. (2010), we acknowledge that NM data with a wide range of location and cutoff rigidity are needed to characterize a GLE including the proton spectrum (e.g. Tylka and Dietrich 2009; Matthiä et al. 2009). Even for simpler quantities such as the onset time and peak flux, it is important to find a NM whose asymptotic look angle is nearly aligned with the interplanetary magnetic field. Such a NM with a low ($\lesssim 1$ GV) cutoff rigidity is expected to give the earliest onset and highest increase in count rate. For example, Shea and Smart (2012) give these NMs for all the GLEs in Solar Cycle 23. The Oulu NM is chosen for seven of the 16 GLEs. Different stations are chosen for the remaining GLEs, and all of them have the rigidity of 1 GV or less.

It is of interest to compare the time profiles of the NM count rates with those of the proton fluxes directly measured from space. The highest-energy measurement of protons from space is achieved by the High Energy Proton and Alpha Detector (HEPAD; Onsager et al. 1996) on the Geostationary Operations Environmental Satellite (*GOES*), which provides differential fluxes in three channels between 350 MeV and 700 MeV, and integral flux above 700 MeV. Figure 1 gives such a comparison of the HEPAD P9 (420–510 MeV) data with the NM data that recorded the earliest onset and/or the highest peak count. The HEPAD data in five-minute average are available at the National Geophysics Data Center.² Note that the

¹<http://cosmicrays oulu.fi>.

²<http://goes.ngdc.noaa.gov/data/avg/>.

Table 1 GLE events and associated flares and CMEs (adopted from Gopalswamy et al. 2010)

GLE			Flare		CME		
Onset		Max	GOES			POS	Width
ID	Date	Time ^a	Int (%) ^a	Class	Location	speed (km/s)	(degs)
55	1997/11/06	12:10	11.3	X9.4	S18W63	1556	360
56	1998/05/02	13:55	6.8	X1.1	S15W15	938	360
57	1998/05/06	08:25	4.2	X2.7	S11W66	1099	190
58	1998/08/24	22:50	3.3	X1.0	N35E09	_{-b}	_{-b}
59	2000/07/14	10:30	29.3	X5.7	N22W07	1674	360
60	2001/04/15	14:00	56.7	X14	S20W85	1199	167
61	2001/04/18	02:35	13.8	C2.2	S20W116	2465	360
62	2001/11/04	17:00	3.3	X1.0	N06W18	1810	360
63	2001/12/26	05:30	7.2	M7.1	N05W54	1446	>212
64	2002/08/24	01:18	5.1	X3.1	S02W81	1913	360
65	2003/10/28	11:22	12.4	X17	S18E18	2459	360
66	2003/10/29	21:30	8.1	X10	S18W04	2029	360
67	2003/11/02	17:30	7.0	X8.3	S18W57	2598	360
68	2005/01/17	09:55	3.0	X3.8	N14W25	2547	360
69	2005/01/20	06:51	277.3	X7.1	N14W61	3242 ^c	360
70	2006/12/13	02:45	92.3	X3.4	S06W23	1774	360

^aAccording to the Oulu Neutron Monitor

^bNo SOHO LASCO data

^cFrom Gopalswamy et al. (2010). There are different estimates (see Grechnev et al. 2008)

1 GV rigidity cutoff corresponds to the proton energy of ≈ 430 MeV, so we expect protons in the P9 channel to overlap with those detected by ≤ 1 GV NMs.

In Fig. 1, the time profiles are plotted in a time range between 10 minutes before and 110 minutes after the onset of the associated flare. Here we are interested only in the general temporal behavior of GLEs at their onsets, so we do not go through the procedures necessary to correct proton spectra from the HEPAD data (see Smart and Shea 1999). Differences among the HEPAD data from different *GOES* satellites are also beyond the scope of these comparisons; data from the “primary” satellite should be official.

In most GLEs we confirm that the NM and HEPAD onset times agree to 10 minutes. Furthermore, the onset times from the Oulu NM are generally within five minutes of those that are earliest. GLEs 65 and 66 are the only exceptions. In contrast, the peak fluxes are often significantly smaller at Oulu than at those NMs that record the earliest onsets (e.g., GLEs 59, 60, and 69).

There are two weak GLEs that may be problematic. While the GLE proton flux usually exceeds 2×10^{-3} ($\text{cm}^2 \text{ s sr MeV}^{-1}$) in the HEPAD P9 channel, GLE 57 appears to have a smaller increase. In GLE 68, it is difficult to find an increase in NM data. The short peak around 10 UT may not be due to particles from the Sun, because both the X-ray flare and the lower-energy proton flux show a slow rise to the peak. Note that in a recent study of SEP events in Solar Cycle 23, Cane et al. (2010) indicated that in these events the proton spectra did not extend to the GLE ranges.

Although it is possible that the energy of protons has to be higher than 500 MeV to produce secondary particles, we point out three non-GLE SEP events that have the proton flux in

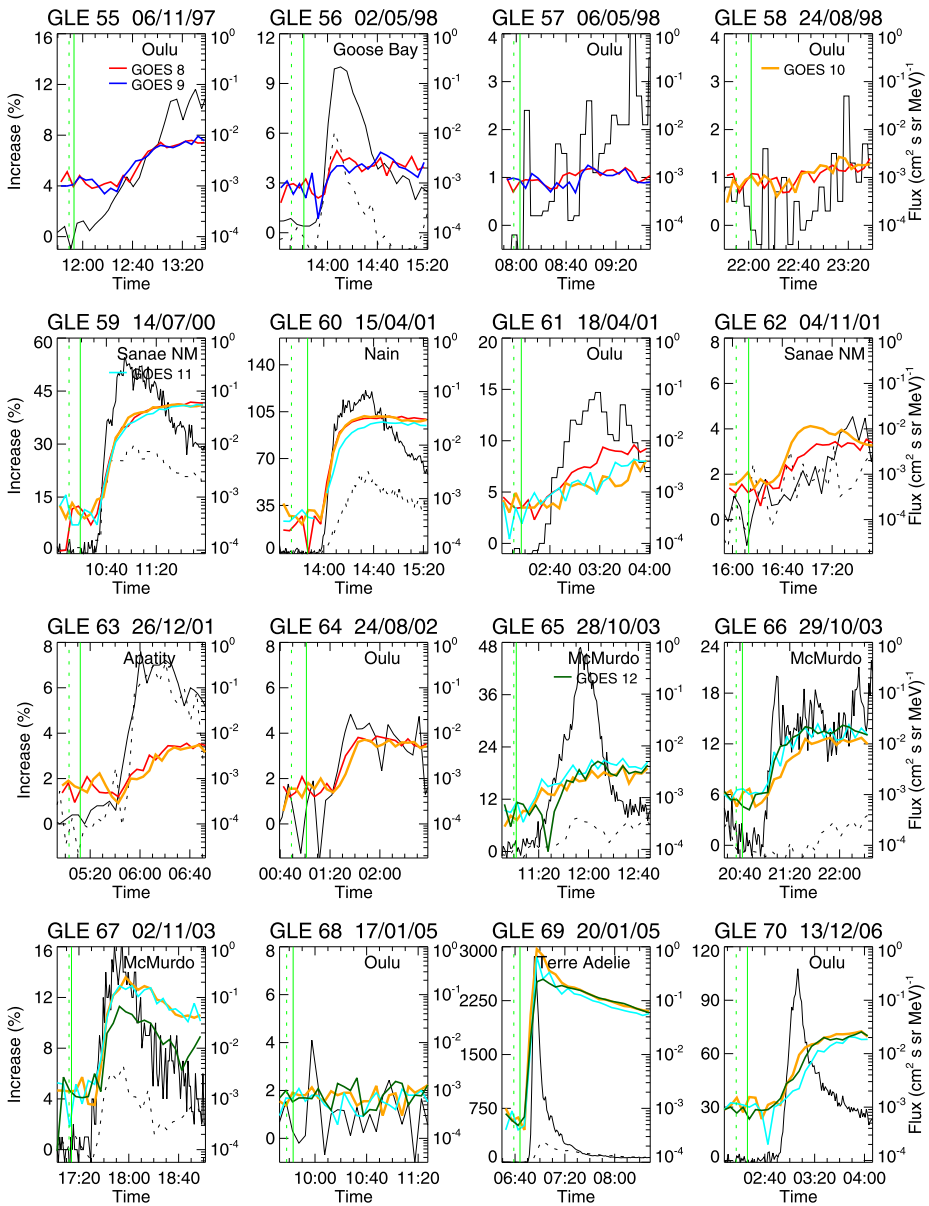


Fig. 1 Comparison of 16 GLEs in Solar Cycle 23 observed by NMs (*in black*) and GOES HEPAD (in color, P9 channel (420–510 MeV)). The latter are from GOES 8 and 9 for GLEs 55–57, GOES 8 and 10 for GLEs 58 and 62–64, GOES 8, 10 and 11 for GLEs 59–61, and GOES 10–12 for GLEs 65–70. The name of the NM is shown. If it is not Oulu, Oulu data are plotted additionally in *dotted lines*. *Green vertical lines* indicate the *onsets* of the associated flare (*dotted line*) and the earliest reported type II burst (*solid line*)

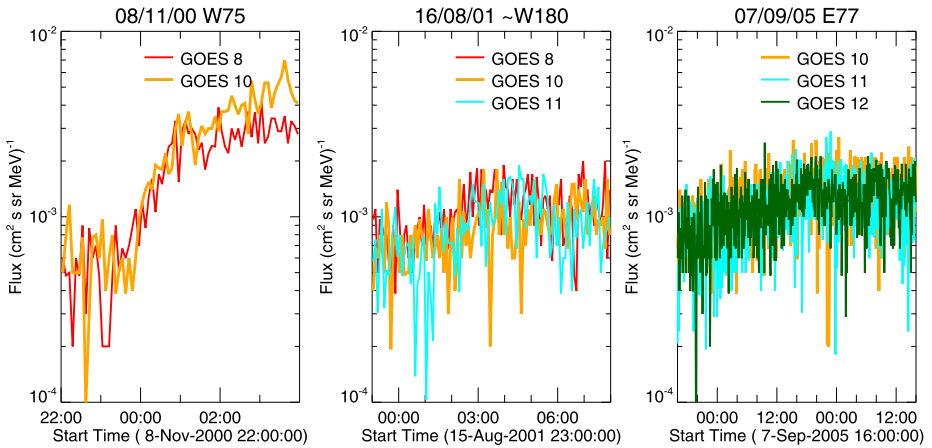


Fig. 2 Examples of non-GLE events with enhanced 420–510 MeV proton flux as observed by GOES HEPAD

P9 channel higher than or at least comparable to that of GLE 57. They are shown in Fig. 2. The 8 November 2000 SEP event represents the third largest >30 MeV proton intensity during Solar Cycle 23 (Mewaldt et al. 2012), and it was produced by a CME from an area between minor ARs (Nitta et al. 2003a). GOES data at 165–500 MeV and 420–510 MeV suggest that this event has a much softer spectrum above ~ 200 MeV than a majority of GLEs. In the two additional events, the proton flux is much smaller and increases on longer time scales. The source longitude of the 16 August 2001 SEP event is believed to be near W180 (Gopalswamy et al. 2002; Cliver et al. 2005), but the >10 MeV proton flux was almost 500 pfu. The AR responsible for the 7 September 2005 event was close to the east limb, and the >10 MeV protons were seen to increase to ~ 100 pfu during the first 24 hours. It is not clear how NMs could observe small events with gradual time profiles, since the relation of the asymptotic look angle of a given NM with the interplanetary magnetic field is expected to change at least on a time scale of hours.

These cases indicate that the distinction of GLEs and non-GLE SEP events may not always be clear. Nevertheless, we shall treat the 16 official GLEs during Solar Cycle 23 as special events. While GLEs with high intensity permit us to study their detailed time structures (e.g. Moraal and McCracken 2011), it is difficult even to find the onset time if the increase is much less than $\sim 10\%$ as in GLEs 57, 58 and 68. For completeness, however, we keep all the GLEs in Table 1 for discussion in the following sections.

3 Properties of the Flares and CMEs Associated with GLEs

Apart from a small number of unusual cases (Cliver 2006), GLEs tend to be associated with intense flares and energetic (fast and wide) CMEs (Gopalswamy et al. 2010, 2012). Here we show that they do not serve as sufficient conditions for GLEs. Columns 5–6 of Table 1 show the peak flux and location of the flares associated with GLEs. It is a common practice to characterize a flare in terms of its soft X-ray ($1\text{--}8\text{ \AA}$) peak flux as measured by the GOES X-ray Spectrometer (XRS). Except for GLE 61, whose source region is estimated to be $\sim 26^\circ$ behind the west limb (see Hudson et al. 2001), all the remaining 15 GLEs are associated with flares above the M7.1 level ($7.1 \times 10^{-5} \text{ W/m}^2$), and 11 of them are above the X2 level

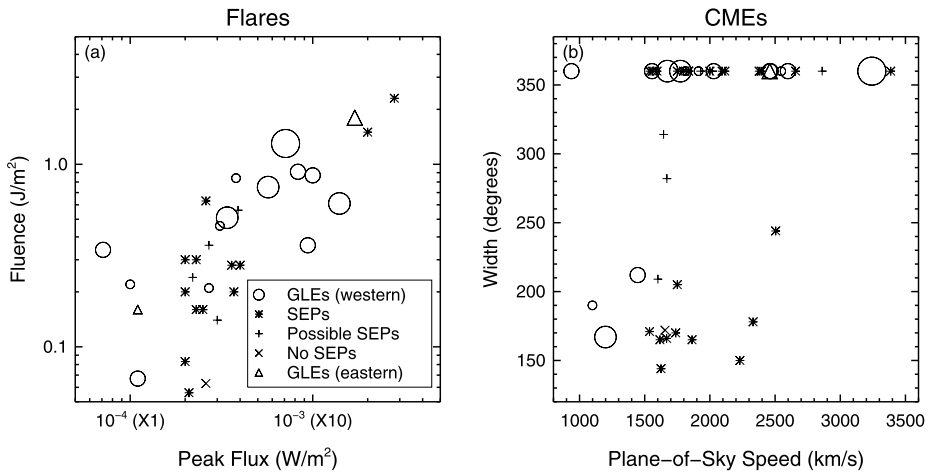


Fig. 3 Scatter plots of two parameters of flares and CMEs that may be correlated with gradual SEPs. Panel (a) include all the 29 flares during Solar Cycle 23 that occurred in the western hemisphere and had the peak flux exceeding the X2 level ($2 \times 10^{-4} \text{ W/m}^2$), three less intense flares associated with GLEs and two flares from the eastern hemisphere. Panel (b) shows 41 CMEs faster than 1500 km/s and wider than 140° from source regions in the longitude range of W00–W120, supplemented by four slower CMEs associated with GLEs and the 28 October 2003 event (the only *triangle*). The data points for GLEs are plotted in four sizes on the basis of the intensities measured by the Oulu NM (see text)

($2.0 \times 10^{-4} \text{ W/m}^2$). We first compare flares associated with GLEs with intense flares in general.

Figure 3(a) is a scatter plot between the X-ray fluxes at the peak and integrated between start and end times (as taken from the NOAA event list), which may be referred to as fluence. The plotted data consist of all the 15 GLEs from disk regions and all the 29 flares during Solar Cycle 23 whose peak flux exceeded the X2 level and which came from the western hemisphere and slightly behind the west limb. The data points for GLEs are plotted in four different sizes on the basis of the Oulu NM peak increase; 1. $<6\%$, 2. $6\text{--}20\%$, 3. $20\text{--}100\%$, and 4. $>100\%$. The count of one NM does not translate to a physical quantity such as the proton flux at a fixed energy range (see Sect. 2). But this designation, as used also in Figs. 3(b), 4 and 7, may give a general idea of the relative magnitudes of our GLEs. The symbol of “possible SEPs” indicates that an SEP event is not clearly isolated due to the residual flux from the previous event. Note that GLEs 58 and 65, plotted in triangles, were from the eastern hemisphere.

There is a good overlap between intense flares and SEP events. For example, if the flare is from the western hemisphere and above the X2 level, it is almost always associated at least with a SEP event. But only 10 of the 29 such flares are associated with GLEs. The two most intense flares are not GLEs; they are the X28 flare on 4 November 2003 at 19:29 UT from AR 10486 located at S19W83, and the X20 flare on 2 April 2001 at 21:32 UT from AR 09393 located at N12W82. Furthermore, four of 15 GLEs are below the X2 level, and there are a number of flares between X1 and X2 (not plotted) that have no SEPs. Although it has been known for a long time that flares that last long, namely long duration events (LDEs), are more intimately associated with CMEs (Sheeley et al. 1975; Kahler 1977), it appears that the fluence is not a much better indicator of GLEs than the peak flux. Part of the reason that the fluence does not make much difference may be that the definition of the

end time as adopted by NOAA, i.e., one half of the peak flux during decay, makes it difficult to distinguish between impulsive flares and LDEs.

Next we discuss whether fast and wide CMEs can serve as sufficient conditions for GLEs. The two rightmost columns of Table 1 give the speed and width of the CMEs as observed by the Large Angle Spectroscopic Coronagraph (LASCO) (Brueckner et al. 1995) on the Solar and Heliospheric Observatory (*SOHO*). Except for the speed of the CME associated with GLE 69, the values are taken from the CDAW CME Catalog (http://cdaw.gsfc.nasa.gov/CME_list). All the CMEs associated with GLEs are (at least partial) halo CMEs with the smallest width of 167° , but the directly measured speeds, projected in the plane of the sky, have a wide range, so do the projection-corrected speeds (Gopalswamy et al. 2010, 2012).

In Fig. 3(b) we compare the CMEs associated and not associated with GLEs in a plot of the width against the plane-of-the-sky speed. In addition to all the 15 CMEs associated with GLEs, we include all the 41 CMEs in Solar Cycle 23 that are wider than 140° and faster than 1500 km/s, with the unambiguously identified source regions in the western hemisphere or less than 30° behind the west limb. A total of ten CMEs are overlapped in the two groups. Four CMEs associated with GLEs are slower than 1500 km/s. They are not special in terms of the locations, i.e., their source regions are not necessarily near disk center, or in terms of the presence of a prior CME, which may help less energetic eruptions be associated with large SEP events (Gopalswamy et al. 2004; Cliver 2006). We therefore conclude that the fast and wide CMEs do not provide sufficient conditions for GLEs, even though many of them are associated with gradual SEP events observed at lower energies, such as the two most intense flares mentioned earlier that are associated with halo CMEs with speeds of 2657 km/s and 2505 km/s, respectively.

4 Basic Properties of the ARs Associated with GLEs

This section considers the possibility that the ARs associated with GLEs may have unique properties. There are 11 ARs that produced the CMEs associated with GLEs during Solar Cycle 23. Table 2 gives their basic properties, i.e., age, sunspot area, magnetic type, detection of sunspot rotation, unsigned magnetic flux near the polarity inversion lines. The age of an AR can be determined quite easily to the time scale of a solar rotation by locating it on synoptic magnetograms in successive Carrington rotations. Most (10/11) of the GLE ARs are less than one solar rotation old, even though some of them survived a few more rotations after the GLEs, such as AR 08100 (see Green et al. 2002). Six of the GLE ARs were seen to emerge on the visible disk, but it was at least a week before a GLE occurred. According to Harvey (1993), the lifetime tends to be longer for larger ARs, and the ARs associated with GLEs tend to be large. Therefore, an old age could have been a discriminating factor for GLE ARs, but most of the GLEs in Solar Cycle 23 occurred in early stages of AR evolution.

Next, we study the sunspot area from the NOAA daily AR list also available in SolarSoft. The fourth column of Table 2 shows the maximum sunspot area during the region's disk passage. One of the GLE regions, AR 10486, which was also the progenitor of severe space weather during the Halloween (October–November) 2003 (Gopalswamy et al. 2005a) period, had the largest sunspot area of all ARs in Solar Cycle 23, but five GLE ARs are smaller than 800 microhemispheres at their maxima. They are even smaller around the times of the GLEs, as shown in the last column of Table 2, which are interpolated from the two measurements closest to the GLE times. Therefore, the large sunspot area does not serve as a discriminating factor for GLEs. According to Gopalswamy et al. (2005a), the sunspot area is less strongly correlated with the SEP intensity and CME speed than with the flare intensity.

Table 2 Basic properties of the 11 ARs associated with GLEs

AR	Date of CM passage	Age ^a	Max area ^b	Mag type	Sunspot rotation	USF PIL ^c	Longitude and (area ^b) at GLE
08100	1997/11/02	<1	1000	β - γ - δ	N	0.35	W63 (840)
08210	1998/05/01	<1	480	β - γ - δ	Y	0.20	W15 (390) W66 (450)
08307	1998/08/26	<1	570	β - δ	N	γ^d	E09 (380)
09077	2000/07/14	<1	1010	β - γ - δ	Y	0.63	W07 (620)
09415	2001/04/09	<1	790	β - γ - δ	Y	0.45	W85 (350) W116 (?)
09684	2001/11/03	<1	550	β - γ - δ	Y	0.18	W18 (510)
09742	2001/12/22	<1	1070	β - γ - δ	Y	0.29	W54 (900)
10069	2002/08/18	2–3	1960	β - γ - δ	Y	0.70	W81 (800)
10486	2003/10/29	<1	2610	β - γ - δ	Y	0.77	E15 (2150) W02 (2250) W59 (2080)
10720	2005/01/16	<1	1630	β - δ	Y	1.04	W25 (1570) W61 (1290)
10930	2006/12/12	<1	680	β - γ - δ	Y	0.32	W23 (680)

^aIn number of solar rotations

^bIn microhemispheres. Corrected for foreshortening

^cAt maximum, in the unit of 10^{22} maxwell

^dNo SOHO MDI data

The parameters in columns 5–7 are more susceptible to foreshortening as the AR approaches the west limb. Therefore the information comes from the time when the AR's longitude was less than 60° . Column 5 shows the magnetic type of the ARs, following the Mt. Wilson classification scheme (Hale et al. 1919; Künzel 1960). It refers to the most complex type the AR undergoes during its evolution. As expected, all the GLE regions have magnetic type that contains δ spots at least during some evolutionary stages. We have also studied sunspot rotation (Brown et al. 2003) for the GLE regions, using white-light images from the Transition Region and Coronal Explorer (TRACE) (Handy et al. 1999) or magnetograms from the Michelson-Doppler Imager (MDI) (Scherrer et al. 1995) on *SOHO*. Although this dynamic phenomenon is frequently associated with major flares (e.g. Nightingale et al. 2005; Zhang et al. 2008; Kazachenko et al. 2009), it is missing or at least unclear in two of the 11 GLE ARs. Moreover, there are many ARs that show sunspot rotation in the western hemisphere but do not accompany gradual SEP events, not to mention GLEs.

Another indicator for major flaring comes from measurements of photospheric magnetic field. One of them is the total unsigned flux (USF) close to the polarity inversion lines (PILs). We identify regions with strong field of opposite polarities tightly packed by multiplying magnetograms that are dilated with a kernel of 3×3 MDI $2''$ pixels (see Schrijver 2007). The flux in maxwell (Mx) is shown rather than Schrijver's parameter R , which is essentially the flux divided by the area corresponding to the MDI pixel (2.2×10^{16} cm²). All the 10 GLE ARs observed by MDI have the USF near the PILs above a threshold of 2×10^{20} Mx, which accounts for 99 % of X-class flares (see Fig. 3 of Schrijver 2007). But many other

Table 3 Comparison of AR parameters (average and standard deviation) in three categories

	GLE regions	SEP regions	δ regions (no SEP)
Sunspot area (microhemispheres)	1102 \pm 621	633 \pm 476	646 \pm 303
Total USF (AR) (10^{22} Mx)	11.9 \pm 5.1	9.0 \pm 4.4	9.5 \pm 3.5
Total USF (PIL) (10^{21} Mx)	4.9 \pm 2.8	3.5 \pm 2.4	2.7 \pm 1.3
Net flux (AR) (10^{22} Mx)	1.5 \pm 0.7	1.7 \pm 1.6	1.2 \pm 1.0
Separation (10^9 cm)	3.8 \pm 2.1	4.7 \pm 2.6	7.0 \pm 2.7

ARs belong to this category, as shown below, so this parameter may not be used to predict GLEs.

Now we compare the properties of ARs that produced GLEs with those of other ARs in a large sample. We have systematically studied the properties of ARs in the mission-long MDI full-disk magnetograms which are sampled every 96 minutes, in a similar manner to the recent study by Mason and Hoeksema (2010). In addition to the ten GLE ARs, we extract a total of 34 regions that produced SEP events (but not GLEs) and 96 non-SEP δ regions in the western hemisphere. Table 3 gives average values of the parameters we are concerned with. They are: the sunspot area, the total USF in the whole region and near the PILs, the net magnetic flux of the whole AR, and the separation of the centroids of the two polarity areas. The parameters for a given region come from the magnetogram in which the unsigned total flux of the whole region is largest while the region is within the $\approx 60^\circ$ longitudinal range. Note that this does not correspond to the GLE time. The sunspot area is again taken from the NOAA daily active region list for the day closest to the magnetogram time.

Figure 4 gives scatter plots of four of the AR parameters in Table 3 (sunspot area, etc.) vs the second (total USF in AR). As in Fig. 3, the data points for GLEs are plotted in four different sizes reflecting the peak intensities in the Oulu NM data. From Table 3 and Fig. 4, the following trends, although not statistically significant, can be found. The GLE ARs have larger sunspot area and total USF both in the whole AR and near the PILs. In contrast, the high net flux may be more characteristic to the SEP regions than to the GLE regions. Finally, the GLE regions tend to be more compact than δ regions without SEPs, even though regions with larger separation tend to produce more intense flares and energetic CMEs (e.g., Guo et al. 2006). Despite the above trends, these basic properties may not be used to distinguish GLEs due to large uncertainties, and more importantly to the time difference between the measurements and the GLEs. There is still a possibility that more advanced observables of ARs can discriminate GLEs. For example, pronounced changes of horizontal magnetic field were reported for AR 10720 just before GLE 69 occurred (Wang et al. 2009). However, these advanced observables were available only for a handful of ARs during Solar Cycle 23.

5 Magnetic Field Connection

In the previous sections, we have shown that neither the magnitude of flares and CMEs nor the basic properties of ARs can be used to distinguish GLEs. Now it is worthwhile to turn to other factors that may contribute to the detection of GLEs. In this section, we discuss the possible importance of magnetic field connection of the source ARs and surrounding

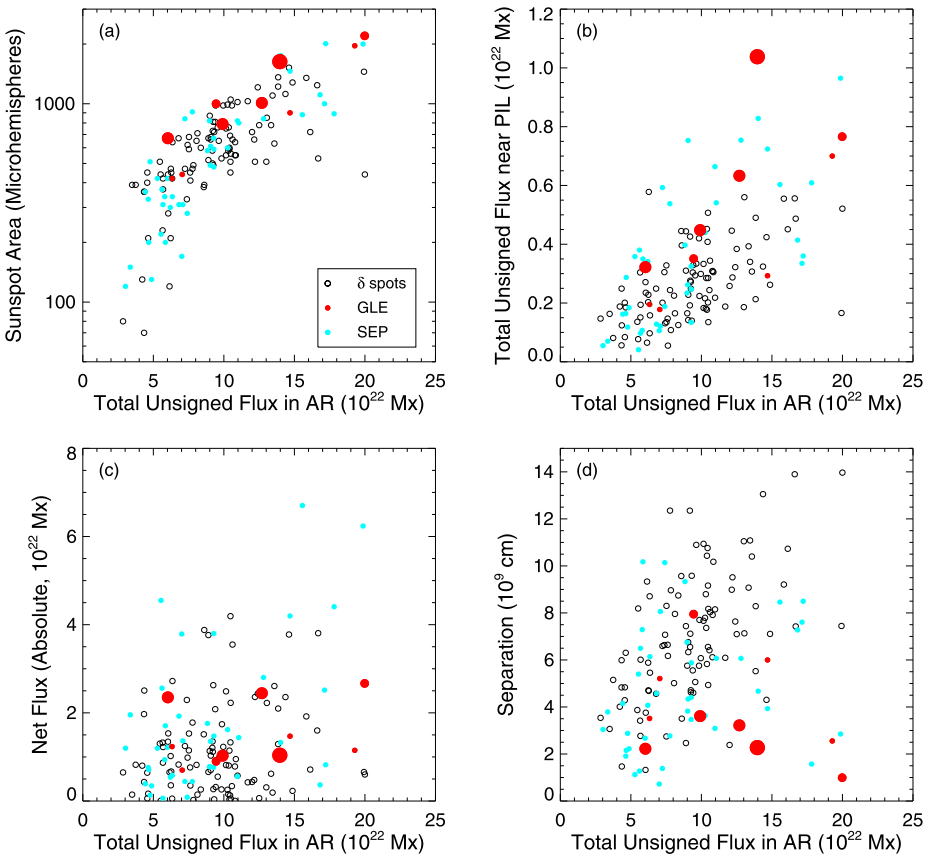


Fig. 4 Four quantities plotted against the total USF of the whole AR, separately for ARs associated with GLEs and non-GLE (lower-energy) SEPs, and δ regions not associated with either of them. They are (a) sunspot area, (b) total USF near PILs, (c) net flux (in absolute value) of the whole region, and (d) separation of the centroids of positive and negative polarity regions. As in Fig. 3, the data points for GLEs are plotted in four sizes on the basis of the intensities measured by the Oulu NM (see Sect. 3)

areas. In the context of SEP events, the western hemisphere, centered around the longitude of W60, is usually thought of as being “well-connected.” This is because the interplanetary magnetic field is approximated as the Parker spiral, and the ends of the field lines that come to the Earth are mapped to the solar longitude of W60 for a typical slow wind speed of ≈ 400 km/s. We expect higher particle flux and quicker onset in SEP events from well-connected regions. At first, we note that some GLEs in Solar Cycle 23 were indeed located around the well-connected longitudes (GLEs 55, 57, 63, 67, and 69). In Table 4, the second column replicates the coordinates of the flares associated with the GLEs. In particular, the flare associated with GLE 69, which had an unusually high flux and quick onset, occurred around W60.

However, as we take into account the observed solar wind speed around the GLE time as shown in the third column of Table 4, the footpoints of the well-connected field lines are sometimes at widely different longitudes (column 4). For example, the difference in longitude between the flare and the footpoint of the well-connected Parker spiral field line (column 5) is now as much as 34° for GLE 69. This would seem to imply that the detection

Table 4 GLEs and magnetic field connection

(1)	(2)	(3)	(4)	(5)	(6)	(7)	(8)	(9)	(10)	(11)
ID	Flare coord. $(\phi, \lambda)_f$	v_{SW} (km/s)	PS long. ϕ_{PS}	Diff. long. $\Delta\phi$	PFSS coord. $(\phi, \lambda)_{PF}$	Dist. Δd lf-PFI	Pol. Sun	Pol. SW	Delay Δt (minutes)	ICME ^b (hours)
55	63, -18	350	65	-2	63, -18	0	M	pM	21	-11
56	15, -15	601	38	-23	14, -17	2	M	M	24	I
57	66, -11	466	50	16	64, -16	6	M	M	27	I
58	-9, 35	423	55	-64	25, 39 ^a	28	P	P	60	N
59	7, 22	604	39	-32	26, 13	20	P	Pm	20	I
60	85, -20	517	45	41	63, -5	26	M	pM	26	-3 ^c
61	116, -20	483	48	68	57, -10	58	M	pM	24	I ^d
62	18, 6	304	74	-57	61, 10	43	M	Pm	57	N
63	54, 5	381	59	-5	60, 12	10	P	pM	27	N
64	81, 2	387	60	21	85, -8	7	M	M	29	N
65	-8, -18	772	29	-37	54, 3	64	M	M	22	+2
66	4, -18	1125	20	-16	14, -14	11	M	P	53	I
67	57, -18	515	44	13	53, -19	4	M	pM	18	N
68	25, 14	678	33	-8	21, 15	4	M	P	17	+3 ^c
69	61, 14	848	27	34	55, 12	6	M	pM	12	+4
70	23, -6	648	35	-12	29, -4	6	M	M	28	N

^aUse Kitt Peak data, because no MDI data are available

^bRefer to Richardson and Cane (2010). “I” and “N” stand for “inside an ICME” and “no ICME”, respectively. The positive (negative) numbers refer to hours after the end (before the start) of the ICME

^cMinor ICME. CME not identified, which is likely from a different region

^dCME not identified, which is likely from a different region

^eCME from a different region (AR 10718)

of GLEs may not depend on the magnetic field connection, as long as we assume that the Parker spiral goes down to the photosphere. However, this picture should not be realistic. We never see coronal images that are dominated by simple radial magnetic field which, in combination with solar rotation, results in the Parker spiral. Images in soft X-rays and EUV reveal the solar corona highly structured with closed loops which likely trace magnetic field lines, and with dark regions, some of which correspond to coronal holes or open field regions. Moreover, the concept of the “well-connected longitudes” ignores the latitudinal excursion of field lines that is needed for a non-ecliptic AR ever to be connected to the Earth.

Here we take another step and conduct a simple modeling of coronal magnetic field, using the potential field source surface (PFSS) model (Altschuler and Newkirk 1969; Schatten et al. 1969). This model assumes that there is no current in the corona below the source surface, usually a sphere of radius $2.5 R_{\odot}$, on which the magnetic field is made radial into interplanetary space. That is, open field lines are those that reach the source surface. Well-connected field lines are a subset of open field lines that intersect the source surface at the ecliptic. We adopt the PFSS model, as implemented into SolarSoft by Schrijver and DeRosa (2003), which is based on the photospheric magnetic maps that are constructed

from (1) MDI data for the area within 60° from disk center and (2) the flux-dispersal model (Schrijver 2001) for the remainder of the solar surface. Such evolving magnetic maps are generated and PFSS extrapolations calculated every 6 hours.

Following Nitta et al. (2006), we trace field lines first from Earth to the source surface assuming the Parker spiral, and then to the photosphere using the PFSS model. We allow for $\pm 7.5^\circ$ and $\pm 2.5^\circ$ uncertainties for the longitude and latitude, respectively, of the source surface coordinates, in an attempt to address possible deviations of the interplanetary magnetic field from the Parker spiral. We identify the field line whose footpoint is closest to the flare. The coordinates $(\phi, \lambda)_{PF}$ of the footpoint of this field line in the photosphere and its distance (Δd) from the flare along a great circle are given in the 6th and 7th columns, respectively. As in the case of impulsive SEP events (see Fig. 8 in Nitta et al. 2006), there are more GLE events in which the footpoint of the field line that connects to Earth is closer to the associated flare than if we assume the Parker spiral all the way to the photosphere (5th column).

In one half of the GLEs, there is a field line whose photospheric footpoint is within 7° from the flare, and whose coordinates on the source surface are consistent with the observed solar wind speed. We may consider these GLEs to be well-connected, including GLE 69. This result suggests that magnetic field connection of the AR may be an important factor for at least certain GLEs. Field lines are traced also upward from the photosphere. Figure 5 shows PFSS extrapolations for four well-connected events on images from the Extreme-ultraviolet Imaging Telescope (EIT) (Delaboudinière et al. 1995) on SOHO. Both the images and the extrapolations refer to times slightly before the GLEs.

In six events, the footpoints of the well-connected field lines are separated from the flare by more than 20° , possibly arguing against the importance of magnetic field connection of the AR to Earth for these GLEs. However, the CME width by the time the CME reaches the source surface is likely to be wider than 20 degrees. In two cases (e.g., AR 9415 for GLEs 60 and 61), open field lines are found close to the flare, as the field is extrapolated from the photosphere, but they intersect the source surface far from the ecliptic. In other cases, no open field lines are found around the AR. These are labeled as occurring in a closed magnetic field environment. In addition to AR 9077 (GLE 59) and 9684 (GLE 62), AR 10486 for GLE 65 belongs to this category.

Figure 6 shows the evolution of large-scale magnetic field around AR 10486. The region is found to be closed until October 29, when we start to see some open field lines of negative polarity (Fig. 6(c)). By the time GLE 67 occurred on November 2, the region was largely open. It is possible that the PFSS model does not properly capture the likely complex magnetic topology of ARs as flare- and CME-prolific as AR 10486, considering its simplifying assumptions of no current in the coronal volume. Moreover, it is a static model, not containing information on dynamics. However, let us for now assume that the PFSS model adequately locates open field lines in areas around the ARs and that these changes reflect the evolution of the ARs and surrounding areas. Of course we are keenly aware of the need to evaluate the PFSS model in individual cases (see, for example Nitta and DeRosa 2008). Incidentally, Liu (2007) found AR 10486 embedded in open field environment, using less frequently updated synoptic magnetic data.

As a consistency check we also compare the photospheric polarity of the open field line closest to the flare and the polarity of the interplanetary magnetic field around the GLE onset. These are given in the eighth and ninth columns of Table 4, where ‘P’ stands for plus (positive or ‘away’ polarity) and ‘M’ stands for minus (negative or ‘toward’ polarity). On the Sun one polarity is assigned by the PFSS model, but at 1 AU, the polarity sometime changes on time scales of ten minutes, not captured in hourly data; we examine high time

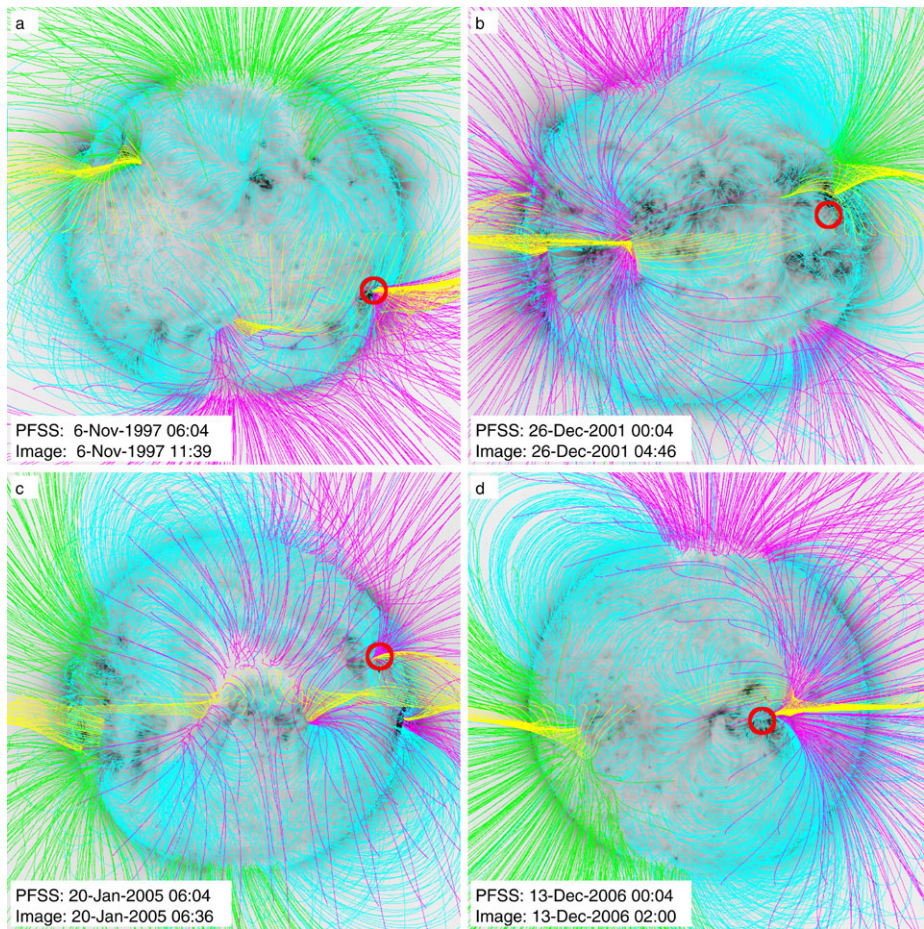


Fig. 5 Extrapolated magnetic field lines plotted on EIT images in reverse color that are taken shortly before four GLEs (55, 63, 69 and 70). The PFSS model is used for extrapolation. *Lines in cyan* are closed field lines, whereas those in *green* and *pink* are open field lines with positive and negative footpoints, respectively. Those in *yellow* are open field lines that are ecliptic at the source surface, a subset of which is expected to be connected to Earth. The locations of the GLE-associated flares are indicated by *circles in red*

resolution data from both Wind and ACE. In such cases, the polarity that lasted longer is shown as upper case. This variation of polarity in the interplanetary magnetic field may indicate departure from a simple Parker spiral, and add another complexity we cannot address within our simple approach. However, we see a general agreement of the polarities at the Sun and 1 AU.

To see the effect of magnetic field connection of the source region on how quickly the GLE starts after the flare onset, we plot in Fig. 7(a) Δd with the time difference Δt of the GLE and flare onsets (column 10 of Table 4). We hardly find a correlation between Δt and Δd . One reason for this may be that the CME associated with the GLE occurs while Earth is within an interplanetary CME (ICME) that results from an earlier CME from the same source region. Then the path length of the field lines that constrain the particles could be longer than the typical Parker spiral (often assumed to be ≈ 1.2 AU long). We use filled

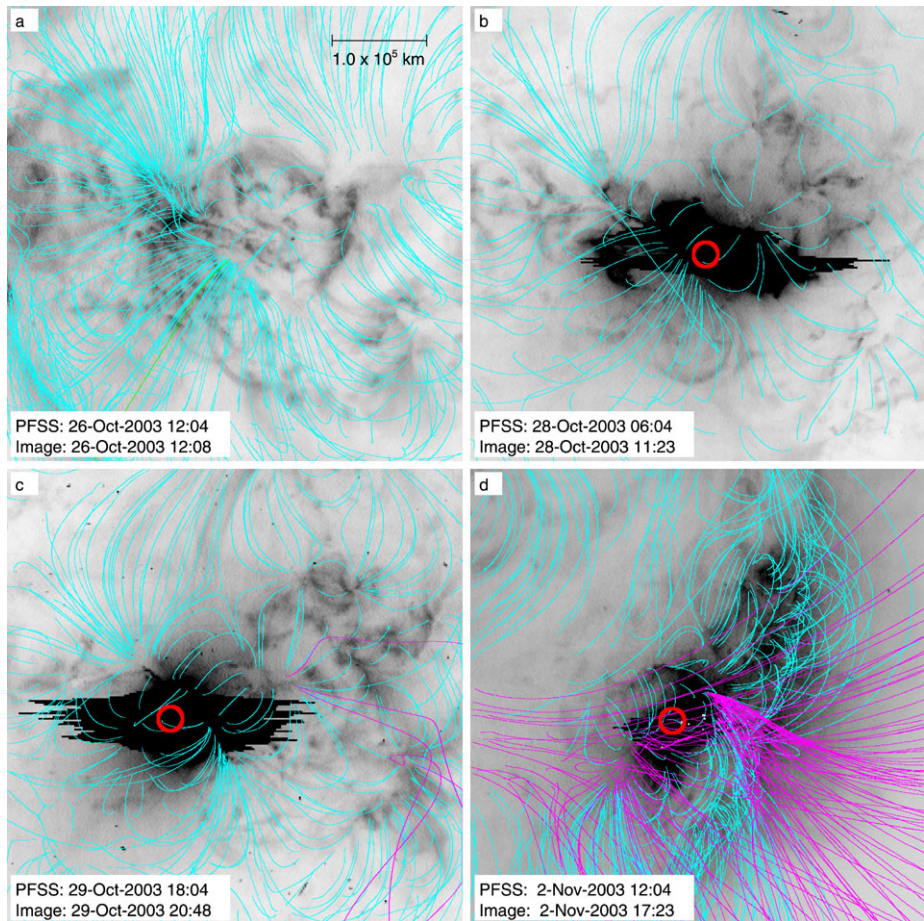


Fig. 6 Magnetic field extrapolation for AR 10486 and the surrounding region at four different times. Field lines are plotted on EIT images taken (a) two days before GLE 65, (b–d) around the times of GLEs 65–67. The same colors are used as Fig. 5 except that ecliptic field lines are not distinguished

circles for these GLEs in Fig. 7(a). In the last column of Table 4 we also indicate those GLEs that were within several hours before or after the passage of an ICME, because interplanetary magnetic field may be disturbed in those time ranges. It may account for GLE 55 ($\Delta d = 0$, $\Delta t = 21$), which appears to come through disturbed interplanetary conditions (the polarity alternating). However, the apparent lack of correlation in Fig. 7(a) will not change if we plot only those GLEs clear of ICMEs. Note that the path lengths for electron events that occur inside ICMEs are not substantially different from those that occur outside ICMEs (Kahler et al. 2011a).

In Fig. 7(b), we plot Δd against the Fe/O ratio, whose enhancement is sometimes thought to be an indicator of flare-accelerated particles. Flares are much less extended than CMEs, so in order for flare-accelerated particles to be injected on to well-connected field lines, these field lines need to be rooted close to the flare. Although a few well-connected events are indeed Fe-rich, no such correlation is seen in the whole sample. The most intense GLE (GLE 69), which is well-connected, is not particularly Fe-rich.

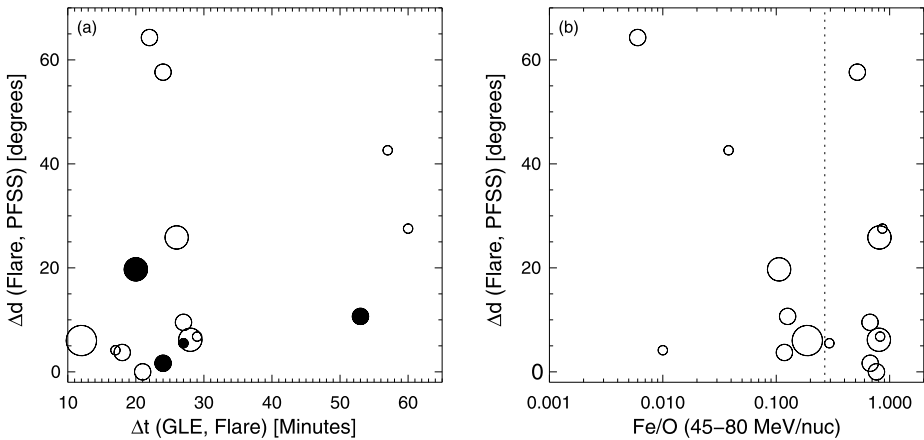


Fig. 7 The relation of the magnetic field connection with (a) the GLE onset time with respect to the flare onset time, and (b) the Fe/O ratio at 45–80 MeV/nuc (from Mewaldt et al. 2012). The right-hand side of the dotted line placed at twice the average SEP value (0.134) of Fe/O (Reames 1995) may define Fe-rich SEP events (Tylka et al. 2005). In (a), filled circles are used for GLEs that were inside an ICME. The data are plotted in four sizes on the basis of the intensities measured by the Oulu NM (see Sect. 3)

6 Large-Scale Coronal Disturbances

What can affect the onset times of GLEs? They are up to an hour after the flare onsets, and these delays are roughly comparable to those of near-relativistic electron events with respect to the associated type III bursts (Krucker et al. 1999; Haggerty and Roelof 2002). Krucker et al. (1999) attributed electron events with delayed onsets, mostly from what were thought to be poorly-connected regions, to the times for coronal waves to propagate from the flare region to well-connected longitudes. Here, coronal waves were represented by EIT waves (Moses et al. 1997; Thompson et al. 1998), which were found to be associated with electron events with delayed onsets, although the waves were too slow to account for relatively short delays.

We now look for EIT waves possibly associated with GLEs by analyzing EIT images. Flares associated with all the GLEs but 58 and 62 were observed by EIT. It turns out that we seldom see clear EIT waves around GLE onsets. In Fig. 8 we show EIT difference images of the same events as Fig. 5. They are typically the first image after the flare onset or the one close to the flare maximum in soft X-rays. In panels (a) and (c), distant areas from the flare appear to be already disturbed, but waves are not found. According to Thompson and Myers (2009), who compiled EIT waves through June 1998, none of the transients associated with GLEs 55–57 are identified with EIT waves with high confidence. If we assume that they start at the flare onset, their speeds are in the range of 500–2000 km/s, depending on where they started. It could be near the flare center or some 10^5 km away as in typical Moreton waves (Moreton and Ramsey 1960; Warmuth et al. 2004). It would have been difficult to observe a wave with a speed of $\gtrsim 1000$ km/s with the typical 12 minute cadence of the EIT. In the event associated with GLE 63 (panel (b)), the large-scale changes cannot be detected with confidence. Therefore a dotted line is used to indicate the possible front. GLE 70 seems to be the only GLE associated with a typical EIT wave whose speed at the bright front is 400–450 km/s as measured in two successive images at 02:36 and 02:48 UT.

In a majority of other GLEs, we see large-scale disturbances without clear EIT wave appearance, similar to panels (a) and (c). The EIT image that shows the change in large

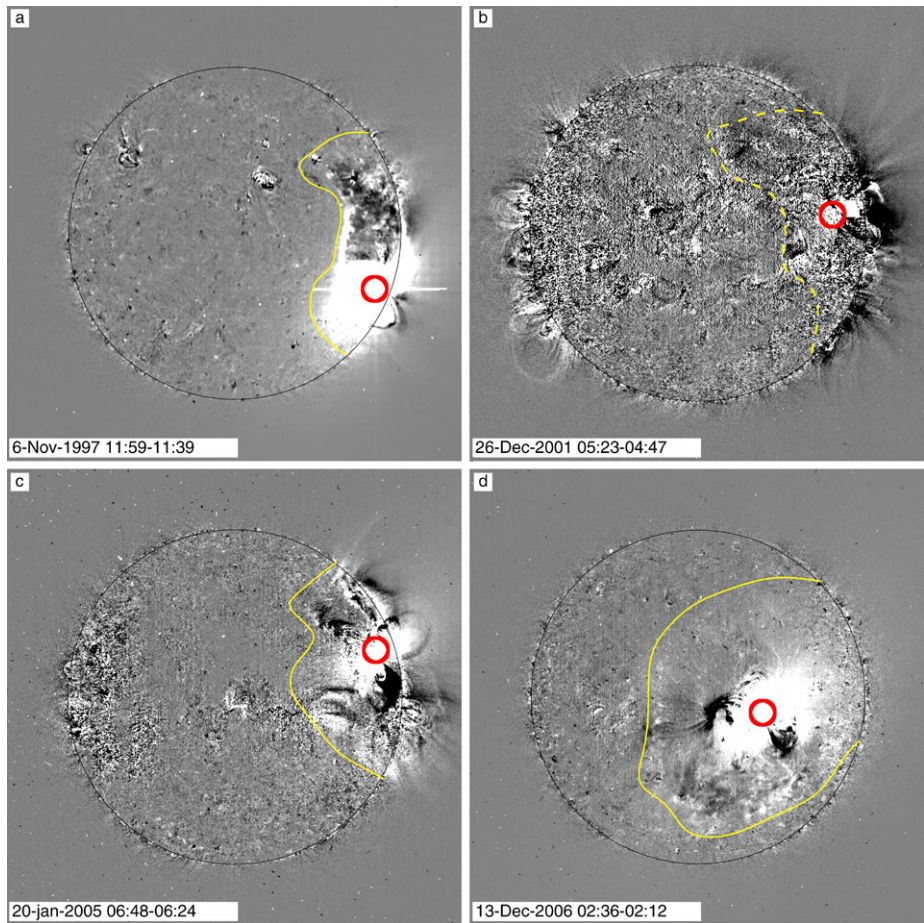


Fig. 8 EIT 195 Å difference images around the flare maximum for the same GLEs as shown in Fig. 5 (55, 63, 69 and 70). The *red circles* mark the flare locations. *Yellow lines* outline what appear to be the fronts of the disturbances. In panel (**b**), a *dotted line* is used because the front is traced only marginally

areas is usually within the time range of the metric type II radio burst as included in the list available at the National Geophysical Data Center (NGDC).³ All the GLEs are associated with metric type II bursts (Gopalswamy et al. 2010, 2012), and in many cases, they are reported by more than one observatories.

However, we do not find it straightforward to isolate metric type II bursts in radio dynamic spectra around the times of GLEs (see White 2012). In Fig. 9, we present them for the same GLEs shown in Figs. 5 and 8. It appears that only panel (b) gives a type II burst clearly from the metric to decametric-hectometetric (DH) ranges (Cliver et al. 2004a). For GLE 70 shown in panel (d), two observatories reported a type II burst to continue to 02:44 UT. But after 02:40 UT a slow drift is seen below 14 MHz, and its metric counterpart is not unambiguously found at earlier times. Other features are also present in the metric range.

³ftp://ftp.ngdc.noaa.gov/STP/SOLAR_DATA/SOLAR_RADIO/SPECTRAL/Type_II/Type_II_1994-2009.

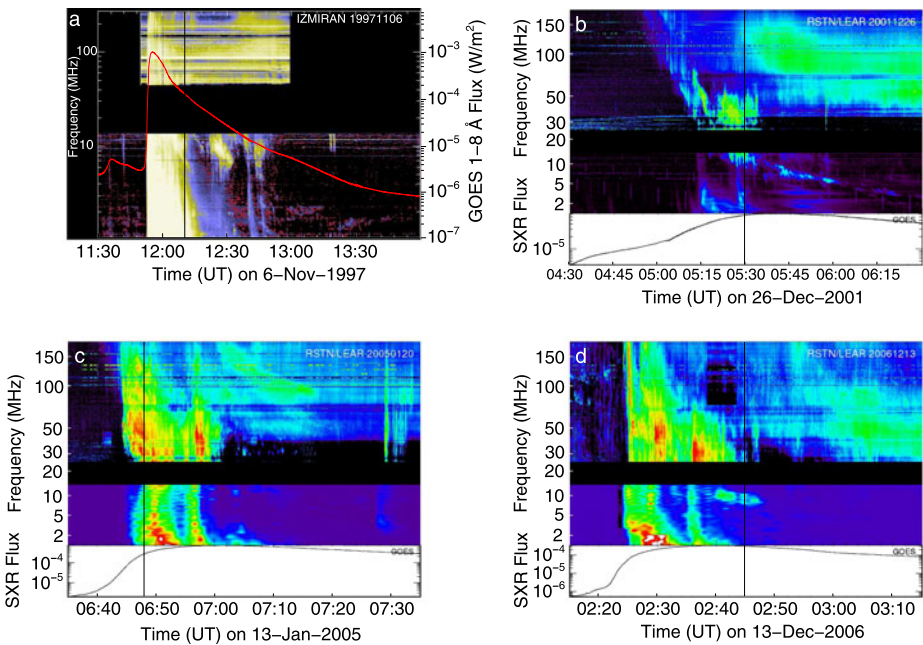


Fig. 9 Radio dynamic spectra of the same four GLEs as Fig. 8 with soft X-ray light curves of the associated flares (courtesy of the Living with a Star Coordinated Data Analysis Workshop in 2002 for (a) and of S. White for (b–d)). The vertical line in each panel indicates the observed GLE onset

Therefore we consider the type II burst in GLE 70 to be marginal. In GLEs 55 and 69 (panels (a) and (c)) the spectra are too complex to allow discrete type II bursts to be identified, suggesting multiple shocks or other processes. This may be related to the large-scale disturbances that typically did not appear as EIT waves. Their presence is not clear in GLE 63, which instead shows the metric type II burst more clearly than others.

Although such large-scale disturbances may play a role in the detection of SEPs with quick onsets from poorly-connected regions such as GLE 65 (whose associated global dimming is discussed by Mandrini et al. 2007), examples such as GLEs 55 and 69 are well-connected events, in which the acceleration region or shock does not have to move large distances before particles are injected. Therefore, we fail to establish the possible importance of coronal or EIT waves in GLEs. A possibility still exists, however, that these large-scale disturbances may bear information on when and where CME-driven shocks form, and become effective in accelerating particles. It has been shown that the CMEs reach the height of $\approx 2 R_{\odot}$ when the shocks accelerate particles (Reames 2009a, 2009b); see slightly different estimates of the CME height by, for example, Kahler (1994) and Gopalswamy et al. (2012). The shocks may form earlier when the CME is at a height of $1.4 R_{\odot}$ as indicated by the onset of metric type II radio bursts (Cliver et al. 2004b; Gopalswamy et al. 2009). The relevance of the large-scale disturbances to CME-driven shocks needs to be investigated in future GLEs using coronal images with high cadence (e.g., Gopalswamy and Yashiro 2011; Gopalswamy et al. 2011) in comparison with the CME development in coronagraph images. In the past CME shocks have been observed in coronagraph images as a streamer deflection or a diffuse region around the CME (Vourlidis et al. 2003; Ontiveros and Vourlidis 2009; Gopalswamy et al. 2009), typically further from the Sun than the height range corresponding to GLE onsets.

Having discussed the difficulty to isolate metric type II bursts in dynamic spectra and to detect coronal waves in EUV and X-ray images for GLEs in the past, we believe that CME-driven shocks are the main ingredient of GLEs. All the GLEs in Solar Cycle 23 were accompanied by DH type II bursts (Gopalswamy et al. 2012).

7 Discussion

The initial task given to us was to find properties of ARs that unmistakably distinguish GLEs. ARs have not been widely discussed in the context of SEP events, and GLEs in particular (Nitta et al. 2003b; Gopalswamy et al. 2005a; Kahler et al. 2011b). From the outset it was not clear if such an attempt could lead to meaningful results. First, the question could be ill-posed unless we know how special GLEs are as compared with other SEP events which also manifest in, for example, >100 MeV protons. In fact, Li et al. (2011) have not distinguished GLEs from SEP events. Similar views of unclear boundaries between GLEs and SEP events are expressed by others (e.g., I. Richardson, private communication 2011). GLEs are registered when secondary particles are detected by ground-based detectors, and it is not straightforward to define GLEs quantitatively in terms of proton flux at certain energies. Direct measurement of protons from space may greatly alleviate this difficulty. However, we are not aware of future plans to measure GeV protons from space. Instead the next-generation *GOES* satellites will have differential proton channels only up to 500 MeV,⁴ down from 700 MeV for the past and present *GOES* satellites. Together with the historical events, this makes ground-based neutron monitors more valuable.

Second, it is likely that CME-driven shock waves directly produce high-energy SEP events (e.g., Reames 1999; Kahler et al. 2011b). Therefore CMEs and their associated flares may contain more direct information on the shock properties than do the source ARs. So we study the general properties of CMEs and flares. Consistent with many studies (e.g., Gopalswamy et al. 2010, 2012), we confirm that GLEs tend to be associated with intense flares and energetic CMEs. But it is difficult to set thresholds that unconditionally distinguish GLEs. Furthermore, we should remember a few GLEs before Solar Cycle 23 that were not associated with major flares (Cliver 2006).

Then we at last study the properties of ARs that may be used to isolate GLEs. One of the most straightforward measures is the age. Old ARs were responsible for GLEs in earlier cycles (Švestka and Simon 1969) and SEPs in general (Belov et al. 2005). However, the GLEs in Solar Cycle 23, with one exception, appeared to come from ARs that are younger than one rotation old. The sample size is yet too small to discuss the possible solar cycle dependence of the origin of GLEs. Next we confirm that the ARs associated with GLEs tend to be magnetically complex, as repeatedly shown in the literature for flare-productive ARs (e.g., Leka and Barnes 2003, and references cited therein). The total unsigned magnetic flux both in the whole AR and near the polarity inversion line (e.g. Schrijver 2007) is higher for GLEs than for other complex ARs. In addition, compared with ARs producing SEP events but not GLEs, GLE ARs tend to be compact. We, however, need to remember that these findings are compromised by various observational restrictions. In order to conduct a statistically study, we only extract the properties of ARs when they were not far from disk center, i.e., not capturing the properties right before the events. The analysis also has large error bars and is subject to a small sample size (especially for GLEs). We have to go beyond the basic properties as presented here to determine if the ARs associated with GLEs are

⁴See <http://www.goes-r.gov/spacesegment/seiss.html>.

really special. We also need techniques to handle ARs close to the limb with vector data (e.g., Wang et al. 2009), so that more useful information on the AR around the time of the GLE can be extracted. For some flare-productive ARs, time variations of vector field have been studied and non-linear force free field extrapolations have been conducted (e.g., Leka and Barnes 2003; DeRosa et al. 2009), but they are still too few to distinguish GLE ARs from others.

The source ARs of GLEs tend to be located in the western hemisphere, which is frequently synonymous with good magnetic field connection to Earth in the context of SEP events including GLEs (see, for example, Kahler et al. 2011b; Gopalswamy et al. 2012). In particular, the flare associated with the most intense GLE, namely GLE 69, occurred around W60, which is often thought to be central in well-connected regions. This leads us to study magnetic field connection of the GLE ARs and surrounding regions, using the PFSS model rather than assuming that the Parker spiral goes straight down to the photosphere. This is now routinely done for impulsive SEP or electron events (Wang et al. 2006; Nitta et al. 2006; Rust et al. 2008). Using the same technique, we find that a half of the GLE ARs are well-connected. We may expect magnetic field connection to influence the onset temporal behavior of SEP events. Indeed we can find a few well-connected GLEs that had a quick onset with respect to the associated flare and CME. However, the GLE onset time is not strongly correlated with how well-connected the AR is. Furthermore, we may also anticipate more flare-accelerated particles from well-connected events as manifesting, for example, in elevated Fe/O ratios (Cane et al. 2003, 2006; Mewaldt et al. 2012). However, apart from a couple of well-connected GLEs with elevated Fe/O ratios, our study indicates that there is hardly a correlation of the Fe/O with magnetic connection.

Following Cliver et al. (1982), we expect injection of particles in a SEP event to begin when the acceleration region first intersects the open field lines connecting to Earth. For the 1 September 1971 GLE, the proton injection nearly coincided with the time an imaged type II burst at 22–55 MHz swept over the footpoint of the nominal Parker spiral connected to Earth (Cliver 1982). Therefore it is important to locate the acceleration region with respect to well-connected field lines. Unfortunately, this could not be done for our GLEs. CME-driven shocks have been observed by LASCO (Vourlidis et al. 2003; Ontiveros and Vourlidis 2009; Gopalswamy et al. 2009), but they are typically further from the Sun than the height range corresponding to GLE onsets. This may partly reflect LASCO's $\gtrsim 20$ minute cadence and lack of coverage below $2 R_{\odot}$ from disk center. The inner coronagraph (COR1) of the Sun Earth Connection Coronal and Heliospheric Investigation (SECCHI; Howard et al. 2008) instrument suite on the Solar TERrestrial Relations Observatory (STEREO; Kaiser et al. 2008) can largely improve this situation (Gopalswamy et al. 2009) for high-energy SEP events during the rising phase of Solar Cycle 24. The stereoscopic view of the origin and propagation of CMEs is extremely useful. This is exemplified by Rouillard et al. (2011), who nicely explained the long delay of a recent non-GLE SEP event with respect to the associated CME, using observations at multiple locations and over large distances in combination with numerical simulations.

In a majority of GLEs, EUV images from the EIT indicate that an extended area far from the flaring AR is disturbed during the impulsive phase of the associated flare. We may imagine this to be caused by coronal waves. However, unlike near-relativistic electron events delayed with respect to type III bursts (Krucker et al. 1999; Haggerty and Roelof 2002), GLEs are seldom associated with clear EIT waves. This can be due to the 12 minute cadence of the EIT, which may leave fast (e.g., $\gtrsim 1000$ km/s) waves undetected. Around the time we find large-scale disturbances, a type II burst is also reported, even though the actual radio dynamic spectrum often appears to be so complex that isolation of the type II

burst is not trivial (White 2012). GLE 63, in which we do not clearly see the large-scale disturbances, instead shows a type II burst from the metric to DH ranges. If the type II burst is a manifestation of the nose of the CME-driven shock, it is possible that the hypothetical fast wave may contribute to the complex dynamic spectrum. Such a wave may result from flare reconnection or represent part of the CME-driven shock away from the nose. Although we could not make a case where a wave like this has to do with a GLE, it is possible that it may correspond to the flank of the CME-driven shock. There we expect efficient particle acceleration, because at the flank quasi-perpendicular conditions may be more naturally met than close to the nose.

We hope to explore the relationship of the CME-driven shock and large-scale disturbances including EIT waves (which need to be redefined), comparing high-cadence images from the Atmospheric Imaging Assembly (AIA; Lemen et al. 2012) on the *Solar Dynamics Observatory* (SDO) with coronagraph images from COR1 and COR2 on STEREO. GLE particles are released when the CME is at the height of $(2-4)R_{\odot}$ (Reames 2009a, 2009b), but this does not necessarily equate with the height of the shock responsible for particle acceleration. AIA has already observed large-scale disturbances as fast as ≈ 1000 km/s, but as of the second half of 2011 no major gradual SEP events, not to mention GLEs, have occurred yet.

With a few channels that include lines forming at high temperatures, the AIA can also observe flare-associated ejections, typically detected in soft X-rays (Shibata et al. 1995). These ejections have been one of the observables used to advocate the “standard” 2-d reconnection model for flares (e.g., McKenzie 2002), although some observational problems of the prototype event have been pointed out (Nitta et al. 2010). In the SEP context, the high Fe/O ratios in gradual SEP events have been shown to be associated with ejections that start without a pre-acceleration phase (Nitta et al. 2003a). The flares that produce these ejections tend to be impulsive and spatially not as extended as others associated, for example, with GLEs 59 and 62 (which have low Fe/O ratios). GLEs 55–57 and 60 belong to this category, but we could not study the possible correlation of flare-associated ejections with the SEP compositions in events after 2001, when *Yohkoh* observations were terminated. AIA data will let us characterize flare-associated ejections in more detail, especially in terms of their relevance to CME-driven shocks and the large-scale disturbances, and eventually to the variable SEP compositions.

Acknowledgements We thank the referees for constructive comments, which have greatly improved the manuscript. This work is supported by NASA grants NNX08AB23G, NNX07AN13G and NNG05GK05G. We are thankful to H. Moraal for providing neutron monitor data, and to M. Shea and D. Smart for enlightening discussions on how these data should be used and interpreted. The authors acknowledge NASA’s Living With a Star program to make possible the Coordinated Data Analysis Workshops on GLEs, without which it would have been much more difficult to analyze relevant data. We used the CME catalog that is generated and maintained at the CDAW Data Center by NASA and The Catholic University of America in cooperation with the Naval Research Laboratory. SOHO is a project of international cooperation between ESA and NASA.

References

- M.D. Altschuler, G. Newkirk, *Sol. Phys.* **9**, 131 (1969)
- M.J. Aschwanden, *Space Sci. Rev.* (2012, this issue). doi:[10.1007/s11214-011-9865-x](https://doi.org/10.1007/s11214-011-9865-x)
- A. Belov, H. Garcia, V. Kurt, H. Mavromichalaki, M. Gerontidou, *Sol. Phys.* **229**, 135 (2005)
- J.W. Bieber, W. Dröge, P.A. Evenson, R. Pyle, D. Ruffolo, U. Pinsook, P. Tooprakai, M. Rujjiwarodom, T. Khumlumlert, S. Krucker, *Astrophys. J.* **567**, 622 (2002)
- D.S. Brown, R.W. Nightingale, D. Alexander, C.J. Schrijver, T.R. Metcalf, R.A. Shine, A.M. Title, C.J. Wolfson, *Sol. Phys.* **89**, 181 (2003)

- G.E. Brueckner et al., *Sol. Phys.* **162**, 357 (1995)
- H.V. Cane, D.V. Reames, T.T. von Roseninge, *J. Geophys. Res.* **93**, 9555 (1988)
- H.V. Cane, T.T. von Roseninge, C.M.S. Cohen, R.A. Mewaldt, *Geophys. Res. Lett.* **30**, 8017 (2003). doi:[10.1029/2002GL016580](https://doi.org/10.1029/2002GL016580)
- H.V. Cane, R.A. Mewaldt, C.M.S. Cohen, T.T. von Roseninge, *J. Geophys. Res.* **111**, A06S90 (2006). doi:[10.1029/2005JA011071](https://doi.org/10.1029/2005JA011071)
- H.V. Cane, I.G. Richardson, T.T. von Roseninge, *J. Geophys. Res.* **115**, A08101 (2010). doi:[10.1029/2009JA014848](https://doi.org/10.1029/2009JA014848)
- E.W. Cliver, *Sol. Phys.* **75**, 341 (1982)
- E.W. Cliver, *Astrophys. J.* **639**, 1206 (2006)
- E.W. Cliver, S.W. Kahler, M.A. Shea, D.F. Smart, *Astrophys. J.* **260**, 362 (1982)
- E.W. Cliver, S.W. Kahler, H.V. Cane, M.J. Koomen, D.J. Michels, R.A. Howard, N.R. Sheeley Jr., *Sol. Phys.* **89**, 181 (1983)
- E.W. Cliver, S.W. Kahler, D.V. Reames, *Astrophys. J.* **609**, 901 (2004a)
- E.W. Cliver, N.V. Nitta, B.J. Thompson, J. Zhang, *Sol. Phys.* **225**, 105 (2004b)
- E.W. Cliver, B.J. Thompson, G.R. Lawrence, A.N. Zhukov, A.J. Tylka, W.F. Dietrich, D.J. Reames, M.J. Reiner, R.J. MacDowall, A.G. Kosovichev, A.G. Lang, in *Proc. 29th In. Cosmic Ray Conf.*, Pune (2005), p. 121
- C.M.S. Cohen, R.A. Mewaldt, R.A. Leske, A.C. Cummings, E.C. Stone, M.E. Wiedenbeck, E.R. Christian, T.T. von Roseninge, *Geophys. Res. Lett.* **26**, 2697 (1999)
- J.-P. Delaboudinière et al., *Sol. Phys.* **162**, 291 (1995)
- M.L. DeRosa et al., *Astrophys. J.* **696**, 1780 (2009)
- N. Gopalswamy, S. Yashiro, *Astrophys. J.* **736**, L17 (2011). doi:[10.1088/2041-8205/736/1/L17](https://doi.org/10.1088/2041-8205/736/1/L17)
- N. Gopalswamy, S. Yashiro, G. Michalek, M.L. Kaiser, R.A. Howard, J.-L. Bougeret, in *Solar-Terrestrial Magnetic Activity and Space Environment*, ed. by H. Wang, R. Xu, COSPAR Colloquia Series, vol. 14, (Pergamon, Boston, 2002) p. 169
- N. Gopalswamy, S. Yashiro, S. Krucker, G. Stenborg, R.A. Howard, *J. Geophys. Res.* **109**, A12105 (2004). doi:[10.1029/2004JA010602](https://doi.org/10.1029/2004JA010602)
- N. Gopalswamy, S. Yashiro, S. Krucker, R.A. Howard, in *Coronal and stellar mass ejections. IAU Symp. 226, IAU*, ed. by K.P. Dere, J. Wang, Y. Yan (2005a)
- N. Gopalswamy, S. Yashiro, Y. Liu, G. Michalek, A. Vourlidas, M.L. Kaiser, R.A. Howard, *J. Geophys. Res.* **110**, A09S15 (2005b). doi:[10.1029/2004JA010958](https://doi.org/10.1029/2004JA010958)
- N. Gopalswamy, W.T. Thompson, J.M. Davila, M.L. Kaiser, S. Yashiro, P. Mäkelä, G. Michalek, J.-L. Bougeret, R.A. Howard, *Sol. Phys.* **259**, 227 (2009)
- N. Gopalswamy, I.H. Xie, S. Yashiro, J. Usoskin, *Indian J. Radio & Space. Physics* **39**, 240 (2010)
- N. Gopalswamy, N. Nitta, S. Akiyama, P. Mäkelä, S. Yashiro, *Astrophys. J.* **744**, 72 (2011). doi:[10.1088/0004-637X/744/1/72](https://doi.org/10.1088/0004-637X/744/1/72)
- N. Gopalswamy, H. Xie, S. Yashiro, S. Akiyama, P. Mäkelä, I. Usoskin, *Space Sci. Rev.* (2012, this issue)
- V.V. Grechnev et al., *Sol. Phys.* **252**, 149 (2008)
- L.M. Green, M.C. López Fuentes, C.H. Mandrini, P. Démoulin, L. van Driel-Gesztelyi, J.L. Culhane, *Sol. Phys.* **208**, 43 (2002)
- J. Guo, H. Zhang, O. Chumak, Y. Liu, *Sol. Phys.* **237**, 25 (2006)
- D.K. Haggerty, E.C. Roelof, *Astrophys. J.* **579**, 841 (2002)
- G.E. Hale, F. Ellerman, S.B. Nicholson, A.H. Joy, *Astrophys. J.* **49**, 153 (1919)
- B.N. Handy et al., *Sol. Phys.* **187**, 229 (1999)
- K.L. Harvey, Ph.D. thesis, Univ. Utrecht (1993)
- R.A. Howard et al., *Space Sci. Rev.* **136**, 67 (2008)
- H.S. Hudson, T. Kosugi, N.V. Nitta, M. Shimojo, *Astrophys. J.* **561**, L211 (2001)
- S.W. Kahler, *Astrophys. J.* **214**, 891 (1977)
- S.W. Kahler, *Astrophys. J.* **428**, 837 (1994)
- S.W. Kahler, *J. Geophys. Res.* **106**, 20947 (2001)
- S.W. Kahler, A. Vourlidas, *J. Geophys. Res.* **110**, A12S01 (2005). doi:[10.1029/2005JA011073](https://doi.org/10.1029/2005JA011073)
- S.W. Kahler, D.K. Haggerty, I.G. Richardson, *Astrophys. J.* **736**, 106 (2011a)
- S.W. Kahler, E.W. Cliver, A.J. Tylka, W.F. Dietrich, *Space Sci. Rev.* (2011b, this issue). doi:[10.1007/s11214-011-9768-x](https://doi.org/10.1007/s11214-011-9768-x)
- M.L. Kaiser et al., *Space Sci. Rev.* **136**, 5 (2008)
- M.D. Kazachenko, R.C. Canfield, D.W. Longcope, J. Qiu, A. DesJardins, R.W. Nightingale, *Astrophys. J.* **704**, 1146 (2009)
- S. Krucker, D.E. Larson, R.P. Lin, B.J. Thompson, *Astrophys. J.* **519**, 864 (1999)
- H. Künzel, *Astron. Nachr.* **285**, 271 (1960)
- K.D. Leka, G. Barnes, *Astrophys. J.* **595**, 1277 (2003)

- J.R. Lemen et al., *Sol. Phys.* **275**, 17 (2012)
- G. Li, G.P. Zank, in *Proc. 29th In. Cosmic Ray Conf.*, Pune (2005), p. 173
- G. Li, R. Moore, R.A. Mewaldt, L. Zhao, A. Labrador, *Space Sci. Rev.* (2011, this volume). doi:[10.1007/s11214-011-9768-x](https://doi.org/10.1007/s11214-011-9768-x)
- Y. Liu, *Astrophys. J.* **654**, L171 (2007)
- C.H. Mandrini, M.S. Nakwcki, G. Attrill, L. van Driel-Gesztelyi, P. Démoulin, S. Dasso, *Sol. Phys.* **244**, 25 (2007)
- J.P. Mason, J.T. Hoeksema, *Astrophys. J.* **723**, 634 (2010)
- D. Matthiä, B. Heber, G. Reitz, M. Meier, L. Sihver, T. Berger, K. Herbst, *J. Geophys. Res.* **114**, A08104 (2009). doi:[10.1029/2009JA014125](https://doi.org/10.1029/2009JA014125)
- K.G. McCracken, H. Moraal, P.H. Stoker, *J. Geophys. Res.* **113**, A12101 (2008). doi:[10.1029/2007JA012829](https://doi.org/10.1029/2007JA012829)
- D.E. McKenzie, in *Proc. the Yokoh 10th Anniversary Meeting, Multi-Wavelength Observations of Coronal Structure and Dynamics*, ed. by P.C.H. Martens, D. Cauffman (Elsevier, Oxford, 2002), p. 155
- R.A. Mewaldt, M.D. Looper, C.M.S. Cohen, D.K. Haggerty, A.W. Labrador, R.A. Leske, G.M. Mason, J.E. Mazur, T.T. von Roseninge, *Space Sci. Rev.* (2012, this issue)
- H. Moraal, K.G. McCracken, *Space Sci. Rev.* (2011, this issue) doi:[10.1007/s11214-011-9742-7](https://doi.org/10.1007/s11214-011-9742-7)
- G.E. Moreton, H.E. Ramsey, *Publ. Astron. Soc. Pac.* **72**, 357 (1960)
- D. Moses et al., *Sol. Phys.* **175**, 571 (1997)
- R.W. Nightingale, Z.A. Frank, T.R. Metcalf, C.A. Kang, in: *AGU/SPD Joint Meeting, Abstract #SP21A-10* (2005)
- N.V. Nitta, M.L. DeRosa, *Astrophys. J.* **673**, L207 (2008)
- N.V. Nitta, E.W. Cliver, A.J. Tylka, *Astrophys. J.* **586**, L103 (2003a)
- N.V. Nitta, E.W. Cliver, A.J. Tylka, P. Smit, in *Proc. 28th In. Cosmic Ray Conf.*, Tsukuba (2003b), p. 3363
- N.V. Nitta, D.V. Reames, M.L. DeRosa, Y. Liu, S. Yashiro, N. Gopalswamy, *Astrophys. J.* **650**, 438 (2006)
- N.V. Nitta, S.L. Freeland, W. Liu, *Astrophys. J.* **725**, L28 (2010)
- T.G. Onsager, R. Grubb, J. Kunches, L. Matheson, D. Speich, R. Zwikl, H. Sauer, in *GOES-8 and Beyond, SPIE Conference Proceedings*, ed. by E.R. Washwell (SPIE, Bellingham, 1996), pp. 281–290
- V. Ontiveros, A. Vourlidas, *Astrophys. J.* **693**, 267 (2009)
- D.V. Reames, *Adv. Space Res.* **15**, 41 (1995)
- D.V. Reames, *Space Sci. Rev.* **90**, 413 (1999)
- D.V. Reames, *Astrophys. J.* **693**, 812 (2009a)
- D.V. Reames, *Astrophys. J.* **706**, 844 (2009b)
- I.G. Richardson, H.V. Cane, *Sol. Phys.* **264**, 189 (2010)
- A.P. Rouillard, D. Odstrčil, N.R. Sheeley Jr., A. Tylka, A. Vourlidas, G. Mason, C.-C. Wu, N.P. Savani, B.E. Wood, C.K. Ng, G. Steinberg, A. Szabo, O.C. St. Cyr, *Astrophys. J.* **735**, 735:7 (2011). doi:[10.1088/0004-637X/735/1/7](https://doi.org/10.1088/0004-637X/735/1/7)
- D.M. Rust, D.K. Haggerty, M. Georgoulis, N.R. Sheeley, Y.-M. Wang, M.L. DeRosa, C.J. Schrijver, *Astrophys. J.* **687**, 635 (2008)
- K.H. Schatten, J.M. Wilcox, N.F. Ness, *Sol. Phys.* **6**, 442 (1969)
- P.H. Scherrer et al., *Sol. Phys.* **162**, 129 (1995)
- C.J. Schrijver, *Astrophys. J.* **547**, L475 (2001)
- C.J. Schrijver, *Astrophys. J.* **655**, L117 (2007)
- C.J. Schrijver, M.L. DeRosa, *Sol. Phys.* **212**, 165 (2003)
- M.A. Shea, D.F. Smart, *Space Sci. Rev.* (2012, this issue)
- N.R. Sheeley Jr., et al., *Sol. Phys.* **45**, 377 (1975)
- K. Shibata, S. Masuda, M. Shimojo, H. Hara, T. Yokoyama, S. Tsuneta, T. Kosugi, Y. Ogawara, *Astrophys. J.* **451**, L83 (1995)
- D.F. Smart, M.A. Shea, *Radiat. Meas.* **30**, 327 (1999)
- Z. Švestka, P. Simon, *Sol. Phys.* **10**, 3 (1969)
- M. Temmer, A.M. Veronig, E.P. Kontar, S. Krucker, B. Vršnak, *Astrophys. J.* **712**, 1410 (2010)
- B.J. Thompson, D.C. Myers, *Astrophys. J. Suppl. Ser.* **183**, 225 (2009)
- B.J. Thompson, S.P. Plunkett, J.B. Gurman, J.S. Newmark, O.C. St. Cyr, D.J. Michels, *Geophys. Res. Lett.* **25**, 2465 (1998)
- A.J. Tylka, W.F. Dietrich, in *Proc. 31st In. Cosmic Ray Conf.*, Łódź (2009)
- A.J. Tylka, C.M.S. Cohen, W.F. Dietrich, M.A. Lee, C.G. MacLennan, R.A. Mewaldt, C.K. Ng, D.V. Reames, *Astrophys. J.* **625**, 474 (2005)
- A. Vourlidas, S.T. Wu, A.H. Wang, P. Subramanian, R.A. Howard, *Astrophys. J.* **598**, 1392 (2003)
- W.-M. Wang, M. Pick, G.M. Mason, *Astrophys. J.* **639**, 495 (2006)
- J. Wang, M. Zhao, G. Zhou, *Astrophys. J.* **690**, 862 (2009)
- A. Warmuth, B. Vršnak, J. Magdalenic, A. Hanslmeier, W. Otruba, *Astron. Astrophys.* **418**, 1101 (2004)
- S.M. White, *Space Sci. Rev.* (2012, this issue)
- J. Zhang, K.P. Dere, R.A. Howard, M.R. Kundu, S.M. White, *Astrophys. J.* **559**, 452 (2001)
- Y. Zhang, J. Liu, H. Zhang, *Sol. Phys.* **247**, 39 (2008)